Integrative transcriptomic analysis unveils FXR as a key regulator of intestinal stemness and inflammation in ulcerative colitis

HAO LIN[1-5*], XINRAN CHENG[6*], YANGYANG REN[7*], YONGMEI ZHANG[2,3], WEIXU CHEN[8], QINGYAN LU[9] and YIQING TIAN[9]

[1]Jiangsu Key Laboratory of Immunity and Metabolism, Xuzhou Medical University, Xuzhou, Jiangsu 221004, P.R. China; [2]Jiangsu Province Key Laboratory of Anesthesiology and Brain Science, Xuzhou Medical University, Xuzhou, Jiangsu 221004, P.R. China; [3]Jiangsu Province Key Laboratory of Anesthesiology, Xuzhou Medical University, Xuzhou, Jiangsu 221004, P.R. China; [4]Department of Gastrointestinal Surgery, Xuzhou Central Hospital, Southeast University, Xuzhou, Jiangsu 221009, P.R. China; [5]Department of Gastrointestinal Surgery, Xuzhou Rehabilitation Hospital (The Affiliated Xuzhou Rehabilitation Hospital of Xuzhou Medical University), Xuzhou, Jiangsu 221003, P.R. China; [6]School of Pharmacy, Anhui Medical University, Hefei, Anhui 230032, P.R. China; [7]Department of Clinical Laboratory, Xinyi People's Hospital, Xinyi, Jiangsu 221400, P.R. China; [8]Department of Gastroenterology, Xuzhou Central Hospital, Southeast University, Xuzhou, Jiangsu 221009, P.R. China; [9]Department of Clinical Laboratory, Xuzhou Central Hospital, Southeast University, Xuzhou, Jiangsu 221009, P.R. China

Received February 6, 2026; Accepted April 24, 2026

DOI: 10.3892/ijmm.2026.5871

Abstract. High-throughput transcriptomic technologies offer a systems-level approach to unravel the mechanisms of complex immune disorders. Inflammatory Bowel Disease (IBD), a classic example of such disorders, involves intricate interactions between genetics, microbiota and immune dysfunction. The nuclear receptor farnesoid X receptor (FXR) is implicated in IBD, but its precise mechanisms remain unclear. To investigate the role of FXR in ulcerative colitis (UC), the present study employed an integrative transcriptomic strategy, combining bulk transcriptomics (GSE75214, GSE13367 and GSE87466) and single-cell RNA-sequencing data (GSE116222) of human UC samples obtained from the Gene Expression Omnibus database. Subsequently, these findings were validated in a dextran sulfate sodium-induced colitis model using FXR global knockout mice. The results revealed that FXR expression is downregulated in UC and co-localizes with the stem cell marker CD133 in intestinal crypts. FXR deficiency exacerbated dextran sulfate sodium-induced colitis, impaired the expression of stemness-associated transcription factors (octamer-binding transcription factor 3/4, homeobox protein NANOG, transcription factor SOX2 and Sal-like protein 4), and activated the NF-κB pathway, leading to increased production of pro-inflammatory cytokines, specifically TNF-α and IL-1β. By integrating bulk and single-cell transcriptomics with genetic validation, the present study uncovered an FXR-dependent mechanism linking intestinal stem cell dysfunction to NF-κB-driven inflammation in colitis, and established a generalizable multi-layer transcriptomic dissection strategy for complex inflammatory disorders.

Introduction

Inflammatory Bowel Disease (IBD) is a group of chronic non-specific inflammatory disorders of the intestine, mainly including ulcerative colitis (UC) and Crohn's Disease (CD) (1). In recent years, with changes in lifestyle (such as the adoption of westernized high-fat diets and increased psychological stress) and environmental factors (including rapid urbanization, increased exposure to pollution and frequent antibiotic use), the global incidence of IBD has continued to rise, particularly in developing countries (2,3). Patients with IBD often present with symptoms such as abdominal pain, diarrhea and mucopurulent bloody stools. The condition is prone to relapse, severely affecting patient quality of life. Certain patients may even progress to colorectal cancer, imposing a heavy burden on healthcare systems (4). Although research on IBD has made some progress, its pathogenesis remains incompletely elucidated. IBD is generally considered to result from the combined effects of multiple factors, including genetic susceptibility, gut microbiota dysbiosis, immune dysfunction and intestinal epithelial barrier damage (5-9). Integrative transcriptomic approaches, particularly the combination of bulk tissue sequencing and single-cell resolution, may facilitate the elucidation of complex molecular networks underlying IBD.

Correspondence to: Dr Yiqing Tian or Dr Qingyan Lu, Department of Clinical Laboratory, Xuzhou Central Hospital, Southeast University, 199 Jiefang South Road, Xuzhou, Jiangsu 221009, P.R. China
E-mail: 824303893@qq.com
E-mail: 910359909@qq.com

*Contributed equally

Key words: ulcerative colitis, farnesoid X receptor, intestinal stem cells, NF-κB, transcriptomics, single-cell RNA sequencing

By investigating these transcriptional layers, researchers can uncover critical cellular crosstalk and identify key regulatory nodes driving the disease.

Farnesoid X receptor (FXR) is a member of the nuclear receptor superfamily, initially discovered as an endogenous ligand receptor for bile acids and playing a central role in regulating bile acid metabolic balance (10). With progress in research, the physiological functions of FXR have continuously expanded, and its roles in maintaining intestinal homeostasis, regulating intestinal epithelial cell proliferation and differentiation, and suppressing inflammatory responses have gained increasing attention (11-13). Abnormal FXR expression has been demonstrated in various intestinal disease models. For example, in dextran sulfate sodium (DSS)-induced colitis and trinitrobenzene sulfonic acid-induced CD models, FXR expression levels are notably reduced, while FXR activation can alleviate mucosal damage by inhibiting intestinal inflammatory responses (14). However, the specific pathological significance of FXR downregulation in colitis and the downstream regulatory networks through which it participates in colitis development require further clarification.

Intestinal stem cells (ISCs), located at the base of intestinal crypts, continuously replenish intestinal epithelial cells through self-renewal and differentiation, maintaining the integrity of the intestinal epithelial barrier. They are a key component in intestinal mucosal damage repair (15). CD133, a transmembrane glycoprotein, is a recognized surface marker of ISCs, and its expression level is closely related to the stemness maintenance and functional activity of ISCs (16). When the intestine suffers inflammatory damage, the proliferative activity of ISCs becomes compromised and their stemness characteristics are markedly diminished, typically manifesting as a decline in self-renewal capacity and the downregulation of essential stemness markers. Impaired stem cell function diminishes intestinal epithelial repair and exacerbates the progression of inflammation (17). Currently, there is limited research on the relationship between FXR and intestinal stem cell function. Whether FXR participates in the pathological process of colitis by regulating intestinal stem cell activity has not been reported.

Uncontrolled inflammation is a core pathological feature of IBD, and the abnormal activation of the NF-κB signaling pathway is considered a key link in the massive release of pro-inflammatory factors (18). Upon activation, the NF-κB pathway can promote the transcription and production of pro-inflammatory factors, such as IL-6 and IL-1β, creating an amplification effect of inflammation and aggravating intestinal mucosal damage (19). Furthermore, stemness transcription factors, such as octamer-binding transcription factor 3/4 (OCT3/4), homeobox protein NANOG, transcription factor SOX2 and Sal-like protein 4 (SALL4), are core molecules maintaining the self-renewal and stemness characteristics of ISCs. Their aberrant expression directly affects stem cell function (20). It has been shown that FXR can modulate inflammation by downregulating the NF-κB signaling pathway and may also positively regulate stemness maintenance (21). However, whether FXR exerts its effects by regulating these stemness factors and inflammation-related molecules in the context of colitis still requires experimental validation.

In the present study, a coordinated transcriptomic investigation was applied to dissect the role of FXR in UC. Bulk transcriptomic data were used for discovery, single-cell transcriptomics were used for cellular resolution, and a genetic mouse model was used for functional validation. The present study not only clarified a key mechanistic pathway in colitis but also demonstrated the utility of a multi-layer transcriptomic framework in deconstructing immune-epithelial interactions.

Materials and methods

Single-cell RNA sequencing (scRNA-seq). All bioinformatics analyses in the present study were performed using R software (version 4.3.3; R Foundation for Statistical Computing). Furthermore, all bioinformatics packages described here and below (including 'harmony', 'edgeR', 'limma', 'DESeq2', 'WGCNA' and 'clusterProfiler') are R-based packages. scRNA-seq data from three human UC samples were downloaded from the Gene Expression Omnibus (GEO) database (https://www.ncbi.nlm.nih.gov/geo/; GSE116222) (22) and processed using the 'Seurat' package (v4.3.0) within the R environment. Data quality was assessed, normalized using the 'NormalizeData' function, and the top 2,000 highly variable genes were identified with 'FindVariableFeatures'. Batch effects were corrected using the 'harmony' package (v1.2.0) (23). Cell clustering was performed with 'FindNeighbors' and 'FindClusters' (resolution=0.8) and visualized via Uniform Manifold Approximation and Projection. Cell types were annotated based on marker genes from the CellMarker database (http://xteam.xbio.top/CellMarker/). Furthermore, the AddModuleScore function implemented in the 'Seurat' package (v4.3.0) was utilized to evaluate the activity of specific signaling pathways (such as the NF-κB pathway) at the single-cell level. This function calculates the average expression levels of a predefined target gene set for each cell, calibrated against the aggregated expression of randomly selected control gene sets.

Bulk transcriptomic analysis. Bulk RNA-seq datasets from control individuals and patients with IBD, including GSE75214 (97 UC, 8 CD and 11 controls) (24), GSE13367 (16 inflamed UC, 18 non-inflamed UC and 20 controls) (25) and GSE87466 (87 UC and 21 controls) (26), were obtained from GEO. Differentially expressed genes (DEGs) in these datasets were identified using the 'edgeR' (v3.40.0), 'limma' (v3.54.0) and 'DESeq2' (v1.38.0) packages in R, with screening criteria of $|\log2FC|>1$ and $P<0.05$ (27-30). The intersection of the results from these methods was calculated using the 'intersect()' function in R, and the overlapping genes were defined as the final DEG set.

Construction of co-expression network. Weighted Gene Co-expression Network Analysis (WGCNA) offers a comprehensive analytical framework for clustering genes sharing analogous expression patterns (31). In the present study, the 'WGCNA' package in R was employed to construct a co-expression network based on the GSE116222 dataset, specifically exploring the association between FXR and

CD133 in intestinal cells. Subsequently, a correlation matrix was generated using the WGCNA package to analyze the association between FXR and distinct modules derived from GSE87466. This specific dataset was selected for WGCNA and subsequent Gene Set Enrichment Analysis (GSEA) because it provides a large, focused cohort strictly comparing UC and healthy controls (n=108). This avoids the confounding disease heterogeneity (such as the presence of CD) or varying inflammatory states present in the other cohorts, thereby ensuring optimal statistical power and biological clarity for network construction and pathway analysis. After selecting an optimal soft threshold (power=8) based on scale-free topology criteria (R^2>0.85), the correlation matrix was transformed into an adjacency matrix, and a topological overlap matrix (TOM) was derived. Genes demonstrating similar expression profiles were clustered into cohesive modules through average linkage hierarchical clustering, employing the TOM-based dissimilarity measure. Modules with a dissimilarity index <0.25 were merged. The modules exhibiting the strongest positive or negative correlations with FXR expression, characterized by the highest absolute Pearson correlation coefficients and showing statistical significance (P<0.05), were selected as the focal points for deeper investigation.

GSEA. The GSE87466 cohort was stratified into high and low expression groups based on median FXR expression. Differential expression analysis was performed using 'DESeq2'. GSEA was then conducted on the entire transcriptome using the 'ClusterProfiler' package, with a significance threshold of P<0.05.

Functional enrichment analysis. Gene Ontology (GO) and Kyoto Encyclopedia of Genes and Genomes (KEGG) pathway enrichment analyses were performed on the key module genes identified via WGCNA. The analyses were conducted using the 'clusterProfiler' package (v4.6.0) in R. The GO database (http://geneontology.org/) was used for annotating biological processes, cellular components and molecular functions, while the KEGG database (https://www.genome.jp/kegg/) was utilized to identify significantly enriched signaling pathways. The threshold for identifying statistically significant GO terms and KEGG pathways was set at an adjusted P<0.05.

Reagents and instruments. DSS (molecular weight, 36-50 kDa) was purchased from MP Biomedicals, LLC. Anti-FXR (cat. no. 25055-1-AP), anti-leucine-rich repeat-containing G-protein coupled receptor 5 (LGR5) antibody (cat. no. 30007-1-AP, for western blotting), anti-CD133 (cat. no. 18470-1-AP), anti-SALL4 (cat. no. 24500-1-AP), anti-TNF-α (cat. no. 17590-1-AP), anti-IL-1β (cat. no. 16806-1-AP) and anti-NF-κB p65 (cat. no. 66535-1-Ig) antibodies were purchased from Proteintech Group, Inc. Anti-LGR5 [cat. no. YM9275, for immunohistochemistry (IHC) and immunofluorescence (IF)], anti-OCT3/4 (cat. no. YM0485), anti-NANOG (cat. no. YM8110) and anti-SOX2 (cat. no. YM9292) antibodies were purchased from ImmunoWay Biotechnology Company. GAPDH antibody (cat. no. AF0006), α-tubulin antibody (cat. no. AF2831) and RIPA lysis buffer (cat. no. P0013B) were purchased from Beyotime Biotechnology. The mouse/rabbit triple-target four-color multiplex immunofluorescence kit (cat. no. RS0035) was purchased from ImmunoWay Biotechnology Company. The kit includes the HRP-polymer anti-rabbit/mouse secondary antibody, 488-labeled Tyramide (green fluorescence), 594-labeled Tyramide (red fluorescence), anti-fade mounting medium with DAPI and high-temperature antibody stripping buffer. The ready-to-use streptavidin-biotin complex-peroxidase Mouse/Rabbit IgG immunohistochemistry staining kit (cat. no. SA1020) (containing a ready-to-use HRP-conjugated universal anti-mouse/anti-rabbit secondary antibody) was purchased from Boster Biological Technology. DMEM high-glucose (cat. no. KGL1211) was purchased from Nanjing KeyGen Biotech Co., Ltd., and penicillin-streptomycin solution (cat. no. VC2003) was purchased from VICMED. The Tanon High-sig ECL Western Blotting Substrate (cat. no. 180-5001) was purchased from Tanon Science & Technology Co., Ltd. A chemiluminescence instrument (Nanjing Zhiheng Intelligent Technology Co., Ltd.) was utilized for gel imaging.

Experimental animals. FXR global knockout (KO; $FXR^{-/-}$) mice (C57BL/6 background) were obtained from Jackson Laboratory. Wild-type (WT) C57BL/6 mice were purchased from GemPharmatech Co. Ltd. All mice were housed in a specific pathogen free-grade animal facility under standard controlled conditions (temperature, 22±2˚C; humidity, 50±10%; 12/12-h light/dark cycle) with *ad libitum* access to standard rodent chow and water. After 1 week of acclimatization, a total of 24 male mice aged 8-10 weeks, weighing 20-22 g, were selected for experiments (n=6 per group). All animal experimental procedures were approved by the Medical Ethics Committee of Anhui Medical University (approval no. LLSC-20232140; Hefei, China).

In vivo functional validation in a genetic model. $FXR^{-/-}$ and WT mice were randomly assigned to control or model groups. Model group mice received 3% DSS in sterile drinking water *ad libitum* for 7 days, followed by normal water for 3 days. Control mice received normal water throughout. Body weight, stool consistency and rectal bleeding were recorded daily. To minimize animal suffering, humane endpoints were established in accordance with ethical guidelines. Criteria for immediate euthanasia included rapid weight loss >20% of the initial body weight, severe lethargy, inability to access food or water or persistent severe rectal prolapse. During the experimental period, no mice met these predefined humane endpoints prior to the scheduled experimental endpoint.

On day 11, mice were euthanized by cervical dislocation. Colon length (cecum to anus) was measured. Mid-colon segments were harvested and briefly washed with cold DMEM (high glucose) supplemented with 1% penicillin-streptomycin to remove fecal contents and prevent bacterial contamination. One part was fixed in 4% paraformaldehyde at room temperature for 24 h, paraffin-embedded and sectioned (4 μm) for H&E staining, IHC and IF, and the other part was snap-frozen in liquid nitrogen for western blotting.

Human sample collection and processing. Human colon tissue samples were prospectively collected from 30 patients at Xuzhou Rehabilitation Hospital (Xuzhou, China) between June 2023 and June 2025. The cohort included 20 patients

with pathologically confirmed active UC and 10 healthy controls. The healthy control samples were obtained from macroscopically normal tissues of patients undergoing screening colonoscopy or surgery for non-inflammatory, non-malignant conditions. The UC group comprised 13 men and 7 women (mean age, 45.6±8.4 years), while the control group consisted of 8 men and 2 men (mean age, 46.2±7.5 years).

The inclusion criteria for patients with UC were confirmed clinical, endoscopic and histological diagnosis of UC. The exclusion criteria included: i) CD or indeterminate colitis; ii) colorectal cancer or other intestinal malignancies; iii) severe systemic infections; and iv) prior treatment with targeted biologics. All procedures were approved by the Medical Ethics Committee of Xuzhou Rehabilitation Hospital (approval no. XK-LW-20230529-014).

IF. Paraffin sections were deparaffinized in xylene, rehydrated in descending ethanol series and subjected to antigen retrieval in 10 mM citrate buffer (pH 6.0) at 100˚C. Endogenous peroxidase was blocked with 3% H_2O_2. Sections were blocked with 5% BSA (Sigma-Aldrich; Merck KGaA) at room temperature for 30 min. Subsequently, multiplex immunofluorescence was performed using the mouse/rabbit triple-target four-color multiplex immunofluorescence kit according to the manufacturer's instructions. Briefly, sections were subjected to sequential staining cycles. In each cycle, tissue sections were incubated overnight at 4˚C with the primary antibody (rabbit anti-FXR at 1:200, rabbit anti-CD133 at 1:150 or rabbit anti-LGR5 at 1:1,000). After washing with PBS containing 0.1% Tween-20, sections were incubated with the kit-provided HRP-polymer anti-rabbit/mouse secondary antibody. The fluorescent signals were then developed using specific fluorophore-conjugated Tyramide substrates (488-labeled Tyramide for green fluorescence or 594-labeled Tyramide for red fluorescence). After signal visualization, the slides were subjected to microwave heating in the high-temperature antibody stripping buffer to remove the bound antibodies before initiating the next staining cycle for the subsequent target. Following the completion of all staining cycles, sections were mounted and nuclei were counterstained simultaneously using the ready-to-use anti-fade mounting medium with DAPI at room temperature. Images were subsequently acquired using a confocal microscope and analyzed with ImageJ software (version 1.54; National Institutes of Health).

Western blotting. Frozen colon tissue was homogenized in RIPA lysis buffer (containing 1% protease inhibitor and 1% phosphatase inhibitor) on ice, followed by centrifugation (12,000 x g, 4˚C, 15 min) and collection of the supernatant. Protein concentration was determined using the BCA method. After adjusting the protein concentration in each sample, 5X loading buffer was added and samples were boiled at 95˚C for 5 nim. A total of 30 μg of protein per sample was subjected to SDS-PAGE and then transferred to a PVDF membrane. Membranes were blocked with 5% skimmed milk at room temperature for 2 h, followed by incubation with primary antibodies (FXR, OCT3/4, NANOG, SOX2, SALL4, TNF-α, IL-1β and NF-κB p65, all at 1:1,000; GAPDH and α-tubulin at 1:1,000) overnight at 4˚C. After washing with TBS containing 0.1% Tween-20 buffer, an appropriate HRP-conjugated secondary antibody (1:5,000; anti-rabbit or anti-mouse depending on the host species of the primary antibody) was applied and incubated at room temperature for 1 h. Signals were visualized using an ECL chemiluminescence kit, and images were captured using a gel imaging system. The gray-scale value ratio of target proteins to the internal reference was quantified using ImageJ software (version 1.54).

Histology and IHC. For histological analysis, paraffin-embedded colon sections (4 μm) were subjected to H&E and periodic acid-Schiff (PAS) staining. For H&E staining, sections were deparaffinized, rehydrated, and stained with hematoxylin for 5 min at room temperature, followed by eosin staining for 2 min at room temperature. For PAS staining, sections were incubated with periodic acid solution for 10 min at room temperature, rinsed with deionized water, and then stained with Schiff reagent for 15 min at room temperature in the dark.

For IHC, paraffin sections were deparaffinized in xylene and rehydrated in a descending ethanol series. Antigen retrieval was performed in 10 mM citrate buffer (pH 6.0) at 100˚C for 15 min, followed by treatment with 3% H_2O_2 for 10 min to block endogenous peroxidase activity. Sections were then blocked with 5% BSA at room temperature for 30 min. Subsequently, sections were incubated overnight at 4˚C with primary antibodies against OCT3/4, SOX2, LGR5 and FXR at 1:200. The kit-provided ready-to-use HRP-conjugated universal anti-mouse/rabbit secondary antibody was applied and incubated for 30 min at room temperature, followed by 3,3'-diaminobenzidine development and counterstaining with hematoxylin for 5 min at room temperature. Representative images were captured using a light microscope (Olympus Corporation).

Statistical analysis. Statistical analysis was performed using SPSS 26.0 software (IBM Corp.), and graphs were plotted using GraphPad Prism 8.0 (Dotmatics). Data are presented as the mean ± standard deviation. Comparisons between two groups were performed using an independent samples Student's t-test. Comparisons among multiple groups were performed using one-way ANOVA followed by Tukey's post hoc test. Correlation analyses between gene expression levels or module eigengenes were evaluated using Pearson's correlation coefficient. $P<0.05$ was considered to indicate a statistically significant difference.

Results

Integrative analysis identifies FXR downregulation as a key feature of colitis. Integrative analysis of bulk transcriptomic datasets (GSE13367, GSE75214 and GSE87466) revealed consistent and significant downregulation of FXR in human UC tissues compared with controls (Fig. 1A-C). Analysis of single-cell data (GSE116222) confirmed this finding at a cellular resolution, showing a gradient of FXR loss from normal to inflamed tissue (Fig. 1D). This cross-omics validation highlighted FXR downregulation as a robust feature of the colitis molecular landscape. To investigate FXR

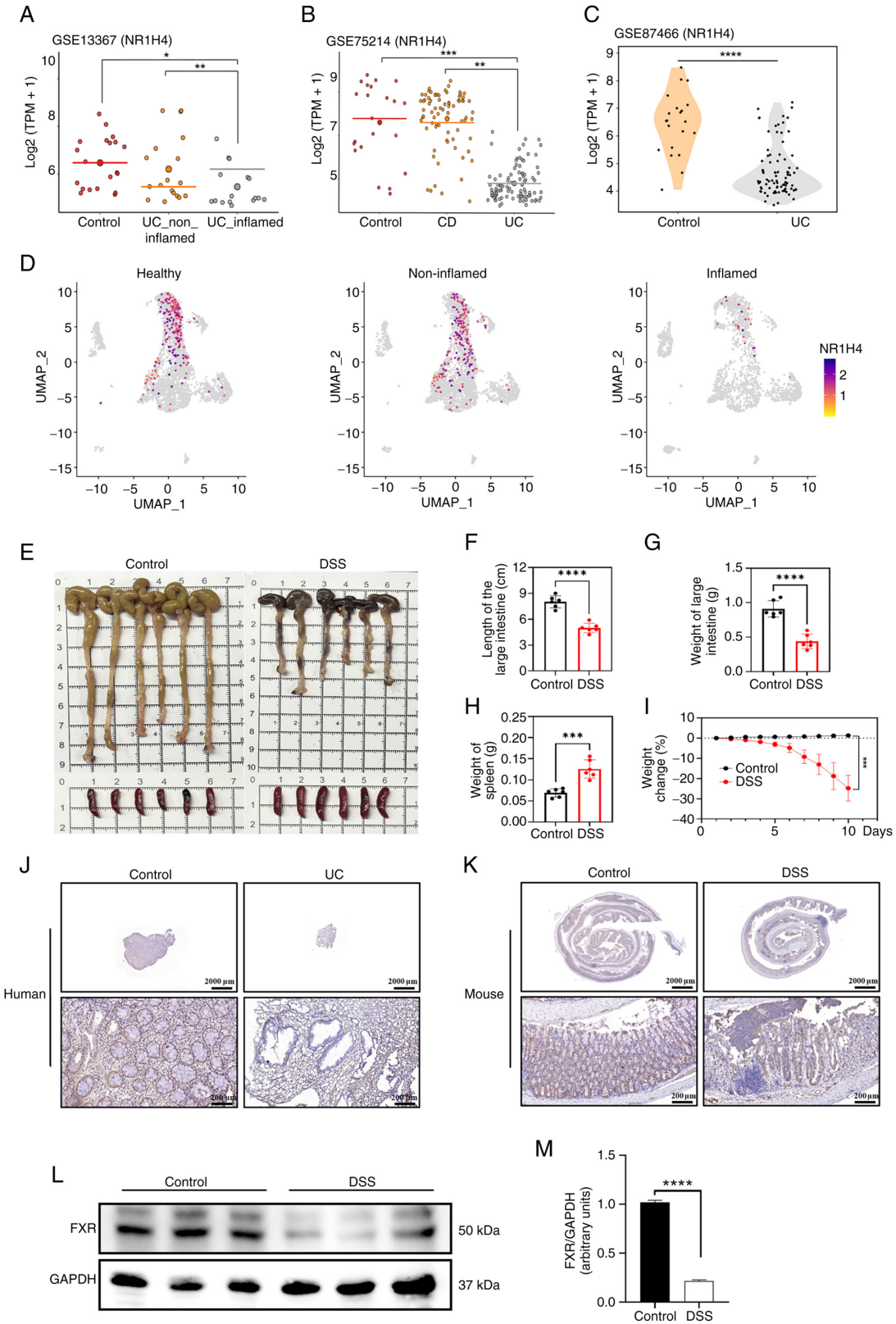

Figure 1. Integrative analysis identifies FXR downregulation as a key feature of UC. Analysis of the bulk transcriptomic datasets (A) GSE13367, (B) GSE75214 and (C) GSE87466 showed significantly lower FXR expression in UC tissues compared with that in controls. (D) Single-cell RNA-sequencing (GSE116222) analysis revealed FXR expression across intestinal cell types. The color key represents the normalized expression level of NR1H4 (the official gene symbol encoding FXR), transitioning from gray (no expression) through yellow and red to dark purple (highest expression). Analysis showed high expression in normal tissue and progressive decrease in inflamed tissue. (E) Representative macroscopic images of the large intestines and spleens from the Control and UC groups. (F) Quantification of the large intestine length. (G) Quantification of the large intestine weight. (H) Quantification of the spleen weight. (I) Body weight loss over time in DSS-treated mice. Immunohistochemistry staining of FXR in (J) human and (K) mouse colon tissues showed reduced FXR-positive cells in the DSS group. Scale bar, 2,000 μm (low magnification); 200 μm (high magnification). (L) Western blot analysis confirmed FXR protein downregulation in DSS-treated mouse colon tissue. (M) Densitometric quantification of FXR protein expression levels relative to GAPDH. Data are presented as the mean ± SD. n=6 per group for macroscopic evaluations and n=3 per group for western blotting. *P<0.05; **P<0.01; ***P<0.001; ****P<0.0001. FXR, farnesoid X receptor; UC, ulcerative colitis; CD, Crohn's disease; DSS, dextran sulfate sodium; UMAP, Uniform Manifold Approximation and Projection; WT, wild-type; TPM, transcripts per million.

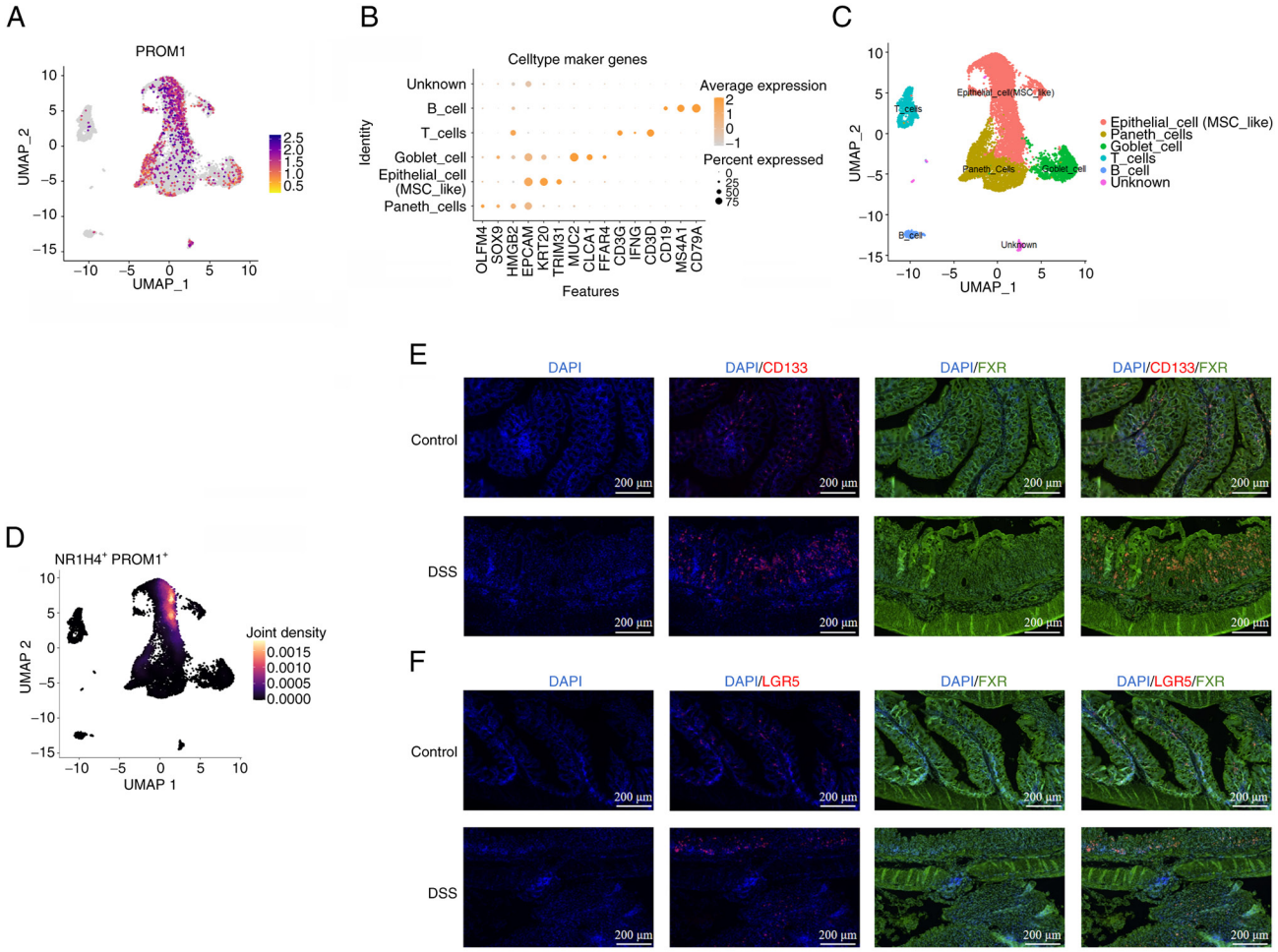

Figure 2. Single-cell resolution maps FXR co-localization to the intestinal stem cell compartment. (A) Single-cell RNA-sequencing (GSE116222) revealed overlapping expression patterns of FXR with the stem cell marker PROM1 (CD133) in UMAP projection. The color key represents the normalized expression level, transitioning from gray (low/no expression) to dark purple (high expression). (B) Cell type annotation based on the CellMarker database identified five major intestinal cell populations, (C) with feature plots showing distribution of marker genes. The dot color represents the average expression level of marker genes (transitioning from light gray for low expression to dark orange for high expression), while the dot size indicates the percentage of cells expressing the respective gene. (D) Co-expression analysis demonstrated correlation between FXR and CD133 in intestinal epithelial cells. The color key indicates the joint expression density of $NR1H4^+$ and $PROM1^+$, transitioning from black (low density) through purple and orange to bright yellow (high density). NR1H4 is the official gene symbol encoding FXR. (E) Immunofluorescence staining of colon tissue from control and DSS mice confirmed co-localization of FXR (green) with CD133 (red) in colonic crypts. Nuclei are counterstained with DAPI (blue). Scale bar, 200 μm. (F) Immunofluorescence staining of colon tissue from control and DSS mice confirmed co-localization of FXR (green) with LGR5 (red) in colonic crypts. Scale bar, 200 μm. Data are representative of three independent experiments. FXR, farnesoid X receptor; DSS, dextran sulfate sodium; UMAP, Uniform Manifold Approximation and Projection; LGR5, leucine-rich repeat-containing G-protein coupled receptor 5; MSC, Marker-defined Stem Cell.

expression *in vivo*, a mouse model of DSS-induced IBD was established. The results showed that the length and weight of the large intestine in the DSS group were both significantly shorter than those of the control group (Fig. 1E-G). The spleen weight in the DSS group increased significantly (Fig. 1H). Concurrently, mouse body weight progressively decreased over time (Fig. 1I). IHC was further used to detect the expression and tissue localization of FXR in human and mouse colon tissue sections. The results revealed that the number of FXR^+ cells and intensity of FXR staining decreased in the UC and DSS groups compared with those in the control groups, indicating downregulation of expression (Fig. 1J and K). Western blot analysis consistently showed downregulation of the FXR protein in DSS-treated mouse colon compared with the control group (Fig. 1L and M). These results demonstrated that FXR expression is downregulated in colitis.

Single-cell resolution maps FXR co-localization to the ISC compartment. While the multi-layer transcriptomic analysis revealed reduced FXR expression in colitis, the precise cellular populations affected remained unclear. Therefore, scRNA-seq data analysis was performed to localize FXR within the intestinal epithelium and assess its co-expression with the stem cell marker CD133 (32). Analysis of the scRNA-seq dataset GSE116222 revealed overlapping expression patterns of FXR with the canonical stem cell marker CD133 (PROM1) (Fig. 2A). Based on the CellMarker database, the single-cell data were annotated and categorized into five major cell types (Fig. 2B and C). Within the epithelial compartment, a CD133-high population was defined within the Marker-defined Stem Cell cluster (MSC_like cluster) and FXR expression was found to be specifically co-localized with this population (Fig. 2D). Simultaneously, immunofluorescence staining of mouse colon tissue revealed

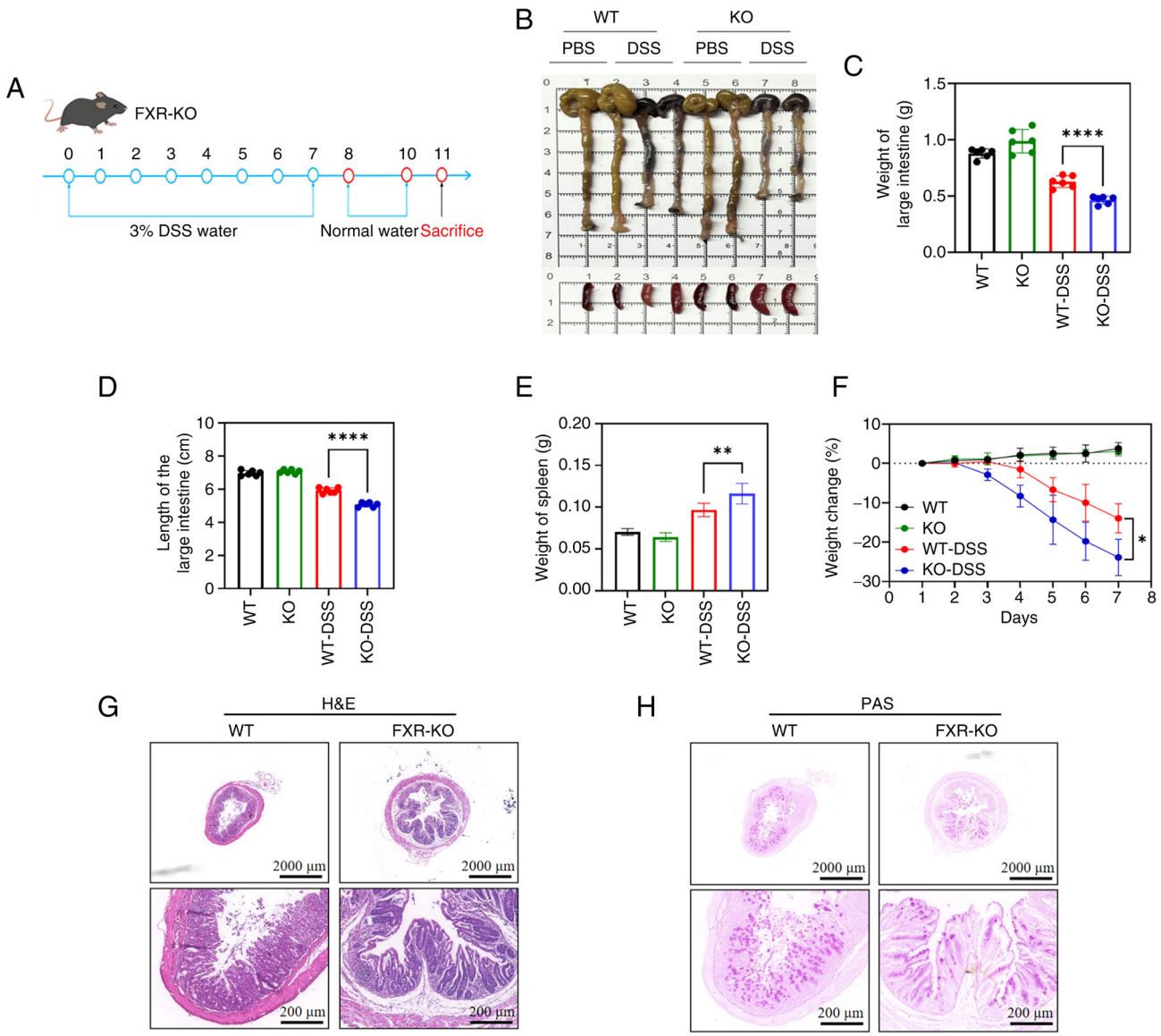

Figure 3. Functional validation in a genetic model confirms the pathogenic role of FXR loss. (A) Schematic of the experimental design for the FXR KO ($FXR^{-/-}$) mouse colitis model. (B) Representative macroscopic images of the colons from WT and $FXR^{-/-}$ mice. (C) Quantification of the colon weight. (D) Shortened colon length in the $FXR^{-/-}$ DSS group compared with that in the WT DSS group. (E) Spleen weight was significantly elevated in the $FXR^{-/-}$ DSS group. (F) Progressive body weight decline over time in $FXR^{-/-}$ DSS mice. Representative images of (G) H&E and (H) PAS staining revealed severe mucosal damage, inflammatory infiltration and gland disruption in $FXR^{-/-}$ DSS colon tissues. Scale bar, 2,000 μm (low magnification); 200 μm (high magnification). Data are presented as the mean ± SD. n=6 per group. *P<0.05; **P<0.01; ****P<0.0001. FXR, farnesoid X receptor; DSS, dextran sulfate sodium; PAS, periodic acid-Schiff; WT, wild-type; KO, knockout.

notable yellow overlapping signals between FXR (green fluorescence) and CD133 (red fluorescence) in colonic epithelial cells, indicating co-localization between FXR and the ISC marker CD133 at the cellular level (Fig. 2E). To definitively confirm the presence of FXR in the crypt base columnar (CBC) stem cell niche, additional *in vivo* validation was performed using the gold-standard ISC marker LGR5 (33). Immunofluorescence staining demonstrated that $LGR5^{+}$ cells were strictly localized to the base of the intestinal crypts (Fig. 2F). Upon DSS-induced injury, a compensatory expansion of $LGR5^{+}$ cells was observed in WT mice, representing a classical mucosal regenerative response. FXR expression exhibited marked co-localization with LGR5 within these CBC cells in DSS-induced mice, supporting its direct regulatory role within the active stem cell niche.

Functional validation in a genetic model confirms the pathogenic role of FXR loss. The $FXR^{-/-}$ mouse model was used to functionally test the hypotheses generated from human omics data. The experimental design for the $FXR^{-/-}$ mouse colitis model is shown in Fig. 3A. Tissue index measurements showed that compared with the WT-DSS group, the KO-DSS group had a markedly decreased colon weight and shortened colon length (Fig. 3B-D). The spleen weight in the KO-DSS group exhibited a substantial increase compared with that in the WT-DSS group (Fig. 3E). Furthermore, the body weight of KO-DSS mice progressively declined over time relative to that of the WT-DSS group (Fig. 3F). H&E and PAS staining results showed that the WT model group exhibited partial epithelial damage and inflammatory cell infiltration in the colonic mucosa. By contrast, the $FXR^{-/-}$ model group displayed severe

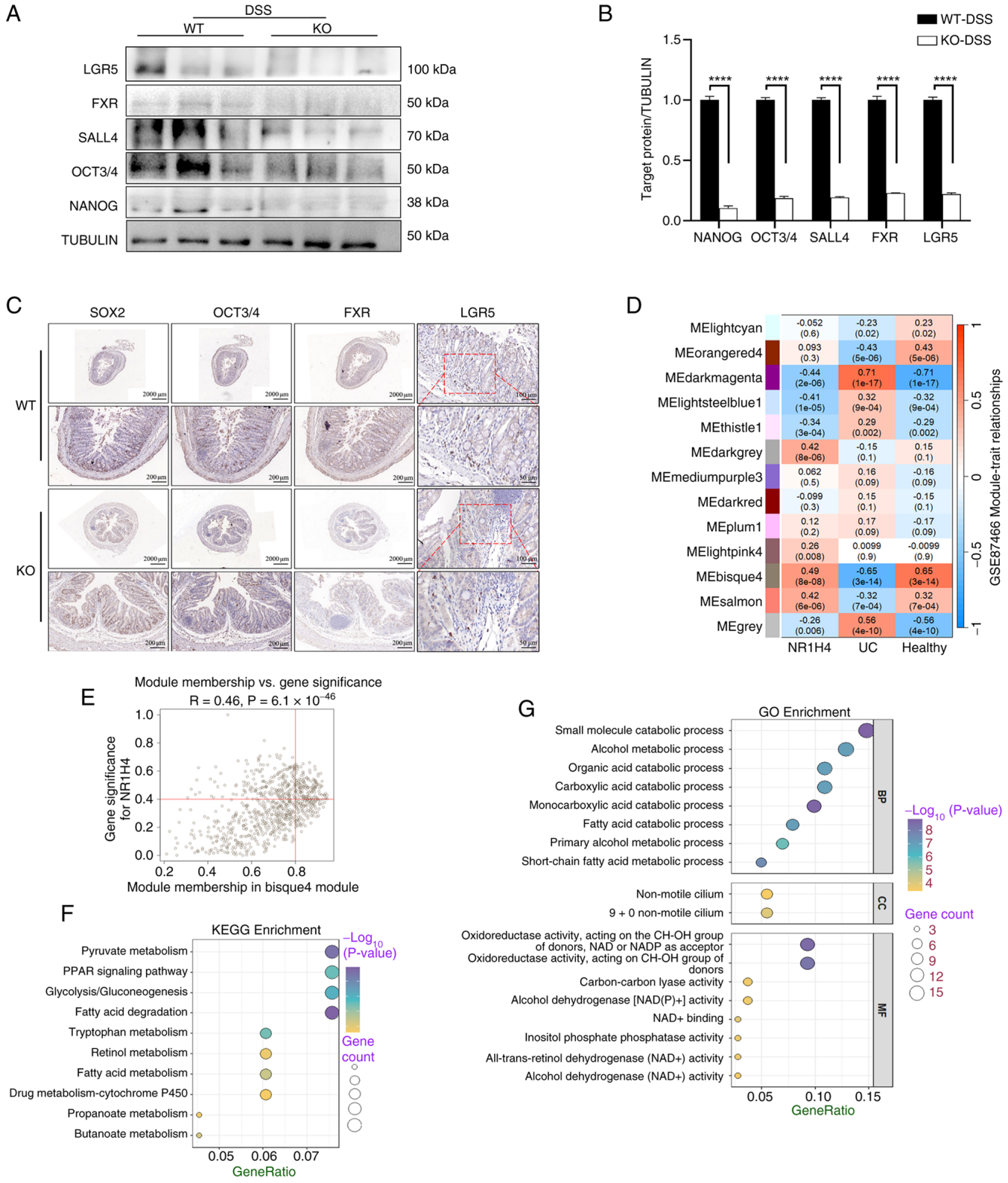

Figure 4. Integrative analysis links FXR to stemness and metabolic pathways. (A) Western blot analysis revealed a notable downregulation of LGR5 and core stemness-associated transcription factors (SALL4, OCT3/4 and NANOG) in colon tissues of FXR$^{-/-}$ DSS mice compared with those of WT DSS controls, reflecting the collapse of the functional stem cell pool and its transcriptional network. (B) Densitometric quantification of protein expression levels. (C) Representative IHC images showing the decreased expression of stemness-associated factors and LGR5 in the epithelial and crypt regions of FXR$^{-/-}$ DSS mice. Scale bar, 2,000 μm (low magnification); 200 μm (high magnification); 100 μm (LGR5 magnification); and 50 μm (LGR5 crypt base high-magnification insets). (D) Weighted Gene Co-expression Network Analysis of the GSE87466 transcriptome identified a gene module (MEbisque4) significantly correlated with FXR expression. The values outside the brackets represent the Pearson correlation coefficients, and the values inside the brackets represent the corresponding P-values. (E) Genes highly correlated with both FXR and the MEbisque4 module were selected. (F) KEGG and (G) GO enrichment analysis of the selected module genes revealed associations with lipid and glucose metabolism pathways. Data are presented as mean ± SD. n=3 per group for western blotting and IHC. ****P<0.0001. IHC, immunohistochemistry; FXR, farnesoid X receptor; DSS, dextran sulfate sodium; WT, wild-type; KO, knockout; LGR5, leucine-rich repeat-containing G-protein coupled receptor 5; OCT3/4, octamer-binding transcription factor 3/4; SALL4, Sal-like protein 4; GO, Gene Ontology; KEGG, Kyoto Encyclopedia of Genes and Genomes; UC, ulcerative colitis; BP, biological process; MF, molecular function; CC, cellular component.

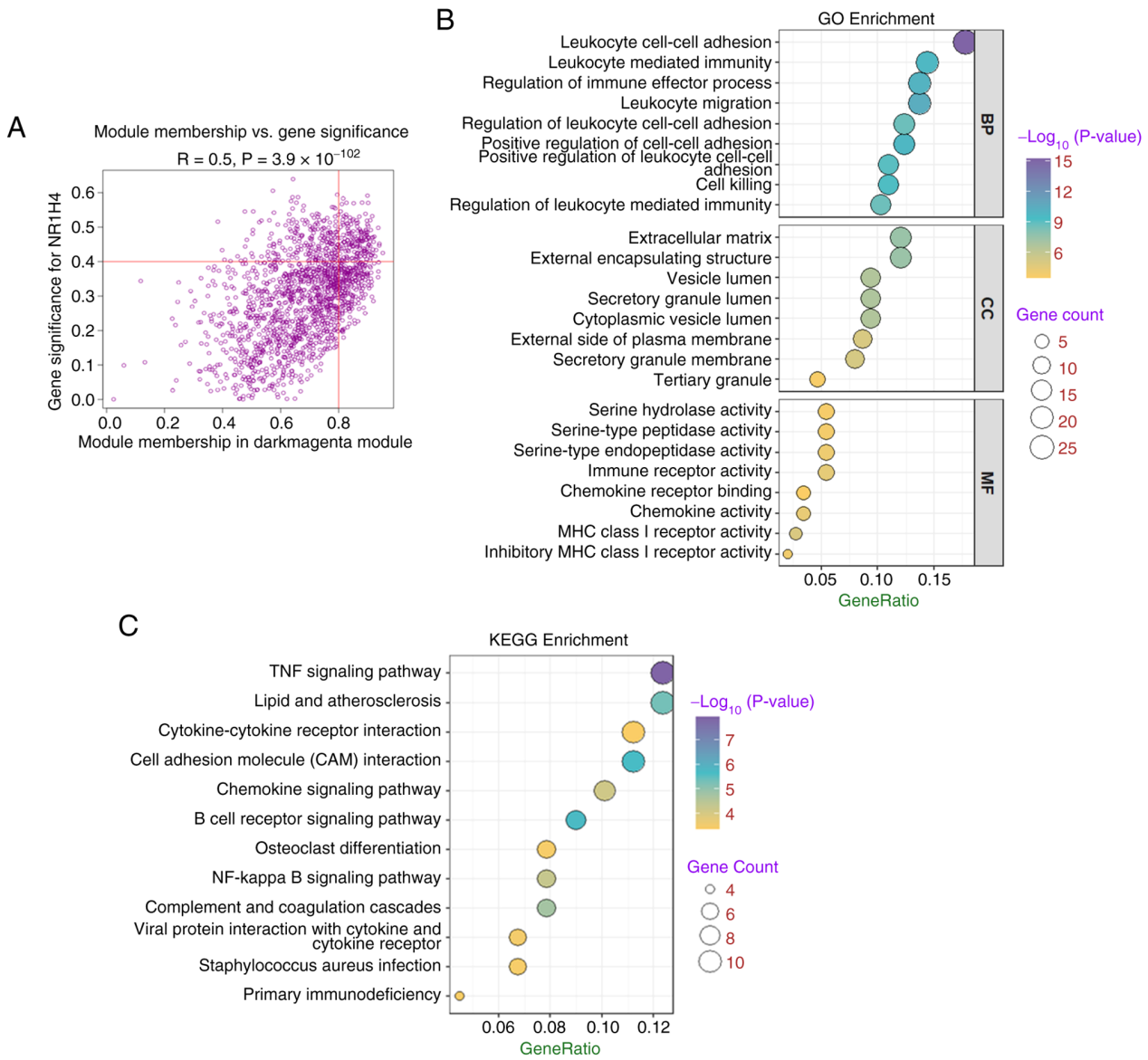

Figure 5. Integrative multi-layer network connects FXR to inflammatory signaling. (A) Weighted Gene Co-expression Network Analysis of the GSE87466 transcriptome identifies a gene module (MEdarkmagenta) negatively correlated with FXR expression. Genes highly correlated with both FXR (negative) and the MEdarkmagenta module were selected. (B) GO enrichment analysis of the selected module genes highlighted immune-related biological processes, including 'leukocyte cell-cell adhesion' and 'leukocyte-mediated immunity'. (C) KEGG pathway analysis showed significant enrichment in 'TNF signaling pathway', 'B cell receptor signaling pathway' and 'NF-κB signaling pathway'. FXR, farnesoid X receptor; GO, Gene Ontology; KEGG, Kyoto Encyclopedia of Genes and Genomes; BP, biological process; MF, molecular function; CC, cellular component.

disruption of colonic mucosal structure, loss of epithelial layer integrity, massive inflammatory cell infiltration in the lamina propria, disorganized or even absent glands and notably aggravated pathological damage (Fig. 3G and H). These results confirmed the central pathogenic role of FXR loss inferred from transcriptional data.

Integrative analysis links FXR to stemness and metabolic pathways. To functionally determine if FXR is required for the maintenance of this stem cell pool during severe inflammation, protein expression levels were assessed in the $FXR^{-/-}$ DSS model. Western blot analysis revealed a notable downregulation of LGR5 protein levels in the colon tissues of $FXR^{-/-}$ DSS mice compared with those of WT DSS controls (Fig. 4A), indicating a failure to maintain the stem cell niche. Consistent with this depletion of the primary CBC stem cell population, notably reduced protein levels of core stemness-associated transcription factors were also observed, including SALL4, OCT3/4 and NANOG in $FXR^{-/-}$ DSS mice (Fig. 4A and B). Consistent with the protein expression data, IHC demonstrated a marked decrease in the positive staining area and intensity for SOX2 and OCT3/4 in the epithelial and crypt regions of the $FXR^{-/-}$ DSS colon (Fig. 4C). Furthermore, high-magnification IHC images confirmed the spatial depletion of the $LGR5^{+}$ population. Specifically, $LGR5^{+}$ signals, which are tightly related to the CBC cells, were diminished in both intensity and cell number compared with those in WT DSS controls (Fig. 4C). This localized loss of the $LGR5^{+}$ pool consistently aligns with the western blot findings, further validating the collapse of the functional stem cell niche upon FXR deletion. Together, these data demonstrated that FXR deficiency leads to the collapse of the ISC pool and its

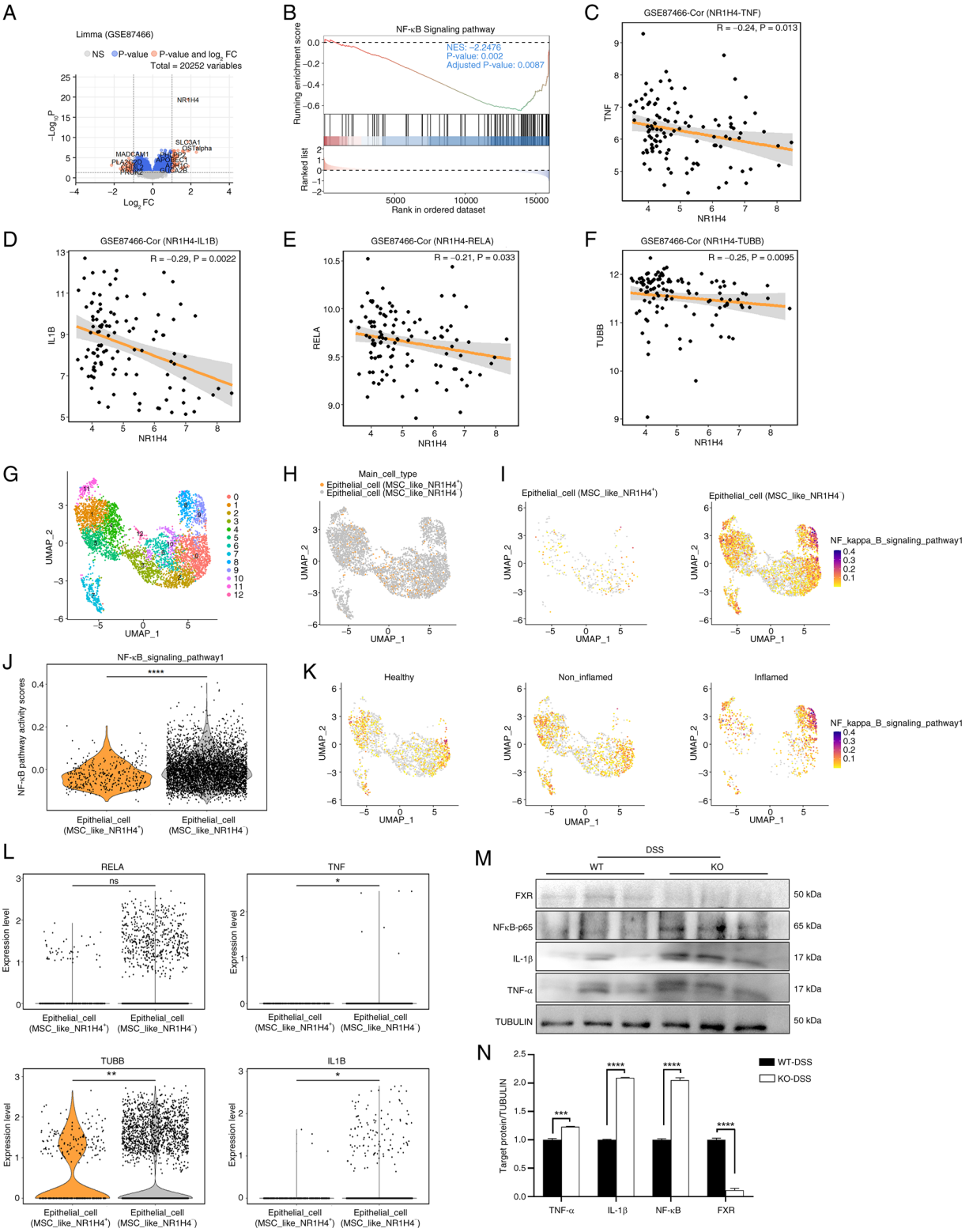

Figure 6. FXR knockout is tightly associated with NF-κB signaling activation and promotes inflammatory responses. (A) Volcano plot of differentially expressed genes between FXR high- and low-expression groups in the GSE87466 cohort. (B) Gene set enrichment analysis showed significant activation of the NF-κB pathway in the FXR-low expression group. Negative correlations between FXR and NF-κB-related genes, including (C) TNF, (D) IL-1β, (E) RELA and (F) TUBB. (G) Sub-clustering of epithelial-related stem cell populations from the single-cell dataset GSE116222 and (H) identification of major subclusters. (I) Stratification of cells into NR1H4^{+} and NR1H4^{-} groups (NR1H4 is the official gene symbol encoding FXR). The color key represents the distribution density of the respective cell populations. (J) NF-κB pathway activity scores calculated using AddModuleScore revealed specific activation in NR1H4^{-} cell populations. (K) Progressive activation of NF-κB signaling from healthy (lowest), through non-inflamed to inflamed (highest). The color key indicates the normalized expression level or pathway activity score, transitioning from low (cool colors) to high (warm colors). (L) Single-cell expression levels of NF-κB-related inflammatory genes in NR1H4^{-} vs. NR1H4^{+} populations. (M) Western blot validation showed notably increased protein levels of TNF-α, IL-1β and NF-κB p65 in colon tissues of FXR$^{-/-}$ DSS mice compared with those in WT DSS controls. (N) Densitometric quantification of protein expression levels. Data are presented as the mean ± SD. n=3 per group for western blotting. *P<0.05; **P<0.01; ***P<0.001; ****P<0.0001. FXR, farnesoid X receptor; DSS, dextran sulfate sodium; WT, wild-type; KO, knockout; UMAP, Uniform Manifold Approximation and Projection; MSC, Marker-defined Stem Cell; NS/ns, not significant; Cor, correlation; NES, Normalized Enrichment Score; FC, fold change.

associated regenerative protein network, thereby impairing mucosal repair.

To explore the broader regulatory network underlying this phenotype, WGCNA was performed on the GSE87466 transcriptome. While multiple modules displayed statistical significance, the MEbisque4 module was specifically selected for downstream analysis because it exhibited the strongest positive correlation with FXR expression (highest correlation coefficient and lowest P-value) (Fig. 4D). This strong positive co-expression indicates that genes within the MEbisque4 module are most tightly co-regulated with FXR, making it the optimal candidate for representing the homeostatic biological functions lost during FXR downregulation in colitis. By applying strict filtering criteria (a Pearson correlation >0.4 with FXR and >0.8 with the MEbisque4 module), 140 core genes were identified (Fig. 4E). Subsequent GO and KEGG enrichment analysis revealed that these 140 genes are enriched in lipid and glucose metabolism pathways (Fig. 4F and G). This transcriptomic profile suggested that FXR may support epithelial stemness and mucosal repair, at least in part, by modulating local cellular metabolism.

Integrative multi-layer transcriptomic network connects FXR to inflammatory signaling. WGCNA of the transcriptome dataset GSE87466 revealed a strong negative correlation between FXR and the MEdarkmagenta module. This suggested that diminished FXR expression may activate specific genes, triggering downstream biological effects. Applying filtering criteria, an absolute Pearson correlation of >0.4 with FXR and >0.8 with the MEdarkmagenta module, 165 key genes were identified (Fig. 5A). Subsequent GO and KEGG enrichment analysis were performed on these 165 genes. GO enrichment analysis revealed that the DEGs were significantly enriched in critical biological processes, including 'leukocyte cell-cell adhesion', 'leukocyte-mediated immunity', 'regulation of immune effector process' and 'regulation of leukocyte cell-cell adhesion' (Fig. 5B). KEGG pathway analysis further demonstrated significant enrichment of the DEGs in pivotal signaling pathways: 'TNF signaling pathway', 'B cell receptor signaling pathway' and 'NF-κB signaling pathway' (Fig. 5C). Collectively, these results underscored that FXR is intimately linked to inflammatory processes.

FXR depletion is tightly associated with NF-κB signaling activation and promotes inflammatory responses. To investigate the relationship between FXR and inflammatory signaling, the GSE87466 cohort was divided into FXR high- and low-expression groups. Differential expression analysis uncovered distinct transcriptional profiles, as illustrated in the resulting volcano plot (Fig. 6A). Subsequently, GSEA was performed, demonstrating marked activation of the NF-κB signaling pathway in the FXR low-expression group (Fig. 6B). Consistently, FXR expression showed negative Pearson correlations with key NF-κB-related genes, including TNF, IL-1β, RELA and TUBB (34,35) (Fig. 6C-F).

To determine the cellular context of this association, sub-clustering analysis was performed on epithelial-related stem cell populations from the single-cell dataset GSE116222 (Fig. 6G and H). Stratifying these cells into FXR^+ and FXR^- groups and scoring NF-κB pathway activity using AddModuleScore revealed specific pathway activation in FXR^- cells (Fig. 6I and J). This activation was progressively elevated across healthy tissues (lowest activation), through non-inflamed tissues (intermediate activation) to inflamed tissues (highest activation) (Fig. 6K), with concomitant upregulation of NF-κB-related inflammatory genes in the FXR^- population (Fig. 6L).

Finally, these findings were validated *in vivo* using the $FXR^{-/-}$ DSS colitis model. Western blot analysis showed notably increased protein levels of TNF-α, IL-1β and NF-κB p65 in $FXR^{-/-}$ colon tissues compared with those in WT controls (Fig. 6M and N), indicating that FXR loss is associated with the hyperactivation of NF-κB signaling and promotes inflammatory responses at the functional level.

Discussion

The present study employed an integrative multi-layer transcriptomic framework to dissect the mechanism of FXR in UC. By sequentially analyzing bulk tissue cohorts, single-cell datasets and a genetically engineered mouse model, observational association was coupled to mechanistic understanding. FXR was identified as a critical molecular node at the intersection of epithelial stemness and immune regulation, whose loss disrupts mucosal repair and induces inflammatory signaling.

The co-localization of FXR with $CD133^+$ ISCs, revealed by single-cell transcriptomics and confirmed spatially, provided a novel cellular context for FXR function. To capture the nuanced dynamics of the ISC niche during inflammatory injury, these findings were further corroborated using the definitive CBC stem cell marker LGR5 (33). Interestingly, WT mice exhibited a compensatory expansion of $LGR5^+$ cells upon DSS-induced injury, a classical mucosal regenerative response where FXR co-localized within the active niche. However, in the absence of FXR, this functional regenerative capacity collapsed. FXR deficiency led to a profound global depletion of the $LGR5^+$ stem cell pool and the concomitant downregulation of core stemness-associated transcription factors (OCT3/4, NANOG, SOX2 and SALL4) (20,36,37). This suggested that FXR is indispensable not merely for the survival of the crypt niche, but for maintaining the transcriptional fidelity and regenerative stemness required for effective mucosal healing. Furthermore, the strong negative correlation between FXR and an inflammatory gene module, culminating in NF-κB activation, illustrated how the loss of a single regulatory factor can destabilize the immune-epithelial interface.

While the present results established a clear association between FXR loss, downregulation of stemness factors and NF-κB activation, the precise causal hierarchy of these events remains to be fully elucidated. It is possible that FXR directly regulates stemness gene expression through transcriptional mechanisms, as FXR response elements have been identified in the regulatory regions of genes involved in cell proliferation in other tissues, such as the Foxm1b gene in regenerating liver tissue (38). Alternatively, the observed stemness impairment may be secondary to the inflammatory milieu created by NF-κB activation, which is known to suppress stem cell function in various epithelial contexts. For example, in the epidermal epithelium, NF-κB signaling induces cell cycle arrest and terminal differentiation, forcing cells to exit the

basal stem cell pool (39). Similarly, in the intestinal epithelium, excessive NF-κB-driven pro-inflammatory cytokines tightly restrict $LGR5^+$ stem cell self-renewal and promote skewed differentiation (40). Elucidating these interconnected pathways will require targeted mechanistic investigations.

The present study demonstrated the utility of an integrative multi-layer transcriptomic framework for deconstructing complex immune-mediated diseases. The workflow, including hypothesis generation from bulk data, cellular deconvolution via single-cell analysis and causal validation in experimental models, provides a reproducible blueprint for investigating other candidate genes or pathways in IBD and related conditions. The identified FXR-stemness-inflammation network represents a high-resolution molecular subtyping of UC pathology that goes beyond conventional histology.

However, several limitations of the current study should be acknowledged. First, regarding the experimental model: The use of global FXR knockout mice, while informative for assessing the role of FXR, does not permit tissue-specific dissection of its function in intestinal epithelial cells vs. immune cells. Generation of conditional knockout mice (such as villin-cre:FXR-flox) would help delineate the cell-autonomous effects of FXR loss in the epithelium. Second, concerning bioinformatic constraints: The present analyses relied on publicly available transcriptomic datasets, which may be subject to batch effects and clinical heterogeneity. Specifically, the scRNA-seq dataset used (GSE116222) includes only three UC samples, limiting statistical power. However, key findings like FXR downregulation and CD133 co-localization were consistently validated in large bulk transcriptomic cohorts and supported functionally *in vivo*. Future studies with larger scRNA-seq cohorts are warranted. Third, regarding mechanistic depth: While the multi-layered data robustly associated FXR deficiency with the hyperactivation of NF-κB signaling, direct mechanistic evidence to confirm whether this regulation is direct or indirect is lacking. FXR may directly bind to regulatory regions of NF-κB target genes, or it may suppress inflammation indirectly via protein-protein sequestration of the p65 subunit. Future studies utilizing chromatin immunoprecipitation assays, combined with *in vivo* rescue experiments using targeted NF-κB inhibitors and FXR agonists (such as GW4064 or obeticholic acid), are required to definitively map this axis. Fourth, regarding systemic metabolism: As FXR is a regulator of bile acid homeostasis, the absence of targeted metabolomic and microbiome profiling is a limitation. The present investigation purposefully focused on the cell-intrinsic role of FXR within the crypt niche. However, it is likely that FXR deficiency exacerbates colitis through dual, parallel mechanisms involving both the localized loss of stemness described in the present study, as well as indirect, systemic effects driven by altered bile acid composition and subsequent gut dysbiosis. Future investigations combining the current transcriptomic framework with rigorous metabolomic profiling will be essential to fully elucidate the complete FXR-centered regulatory network in intestinal inflammation. Furthermore, the potential therapeutic implementation of FXR agonists in UC, while mechanistically promising, requires rigorous evaluation in preclinical models and clinical trials, with careful consideration of both metabolic and immune-modulatory effects.

In conclusion, the present integrative multi-layer transcriptomic analysis established FXR as a guardian of intestinal homeostasis, whose loss disrupts stem cell function and activates pro-inflammatory pathways in colitis. More broadly, the current study served as an example of how coordinated multi-layer transcriptomic strategies can effectively decipher the cellular and molecular circuitry of immune-inflammatory diseases. The mechanistic network delineated in the present study provides a molecular foundation for future investigations into targeted therapeutic interventions in UC and related inflammatory disorders.

Acknowledgements

The authors would like to thank Professor Yuxian Shen from Anhui Medical University for providing administrative support, animal housing infrastructure and the overarching ethical protocol (approval no. LLSC-20232140) that facilitated the *in vivo* experiments conducted by his student, Xinran Cheng, in the present study.

Funding

This work was supported by the Jiangsu Key Laboratory of Immunity and Metabolism (grant no. XZSYSKF2022040), the General Project of Xuzhou Basic Research Plan in 2023 (grant no. KC23070), Xuzhou Municipal Health Commission 2024 Youth Medical Science and Technology Innovation Project (grant no. XWKYHT20240016) and Science and Technology Development Fund of Affiliated Hospital of Xuzhou Medical University (grant nos. XYFM202343 and XYFM202412).

Availability of data and materials

The data generated in the present study may be requested from the corresponding author.

Authors' contributions

YT and QL conceived and designed the present study. HL, XC, YR, WC and YZ performed data curation. HL, XC and QL performed data analysis and interpretation. HL and YR conducted the experiments. HL, XC and YZ developed the methods. QL and YT performed project administration, and YT provided resources. HL and XC performed software analysis. YT, QL and YZ supervised the study. WC performed the experimental validation of the transcriptomic findings using *in vivo* models and molecular assays. HL, XC and YR performed data visualization by generating bioinformatic plots and assembling the manuscript figures. YT and HL wrote the original draft, and all authors reviewed and edited the manuscript. YT and QL confirm the authenticity of all the raw data. All authors read and approved the final manuscript.

Ethics approval and consent to participate

All animal experiments were conducted in accordance with the guidelines of the Animal Care and Use Committee of Anhui Medical University (approval no. LLSC-20232140). All procedures involving human participants were approved

by the Medical Ethics Committee of Xuzhou Rehabilitation Hospital (approval no. XK-LW-20230529-014). Written informed consent was obtained from all participants.

Patient consent for publication

Written informed consent was obtained from all patients prior to their participation in the current study, including consent for publication.

Competing interests

The authors declare that they have no competing interests.

References

1. Yang X, Guo H and Zou M: Inflammatory bowel diseases: Pathological mechanisms and therapeutic perspectives. Mol Biomed 7: 2, 2026.
2. Piovani D, Danese S, Peyrin-Biroulet L, Nikolopoulos GK, Lytras T and Bonovas S: Environmental Risk factors for inflammatory bowel diseases: An umbrella review of meta-analyses. Gastroenterology 157: 647-659.e4, 2019.
3. Estevinho MM, Midya V, Cohen-Mekelburg S, Allin KH, Fumery M, Pinho SS, Colombel JF and Agrawal M: Emerging role of environmental pollutants in inflammatory bowel disease risk, outcomes and underlying mechanisms. Gut 74: 477-486, 2025.
4. Shah SC and Itzkowitz SH: Colorectal cancer in inflammatory bowel disease: Mechanisms and management. Gastroenterology 162: 715-730.e3, 2022.
5. Iliev ID, Ananthakrishnan AN and Guo CJ: Microbiota in inflammatory bowel disease: Mechanisms of disease and therapeutic opportunities. Nat Rev Microbiol 23: 509-524, 2025.
6. Danne C, Skerniskyte J, Marteyn B and Sokol H: Neutrophils: From IBD to the gut microbiota. Nat Rev Gastroenterol Hepatol 21: 184-197, 2024.
7. Foerster EG, Mukherjee T, Cabral-Fernandes L, Rocha JDB, Girardin SE and Philpott DJ: How autophagy controls the intestinal epithelial barrier. Autophagy 18: 86-103, 2022.
8. Chen Y, Cui W, Li X and Yang H: Interaction between commensal bacteria, immune response and the intestinal barrier in inflammatory bowel disease. Front Immunol 12: 761981, 2021.
9. Dong L, Xie J, Wang Y, Jiang H, Chen K, Li D, Wang J, Liu Y, He J, Zhou J, *et al*: Mannose ameliorates experimental colitis by protecting intestinal barrier integrity. Nat Commun 13: 4804, 2022.
10. Won TH, Arifuzzaman M, Parkhurst CN, Miranda IC, Zhang B, Hu E, Kashyap S, Letourneau J, Jin WB, Fu Y, *et al*: Host metabolism balances microbial regulation of bile acid signalling. Nature 638: 216-224, 2025.
11. Chen L, Jiao T, Liu W, Luo Y, Wang J, Guo X, Tong X, Lin Z, Sun C, Wang K, *et al*: Hepatic cytochrome P450 8B1 and cholic acid potentiate intestinal epithelial injury in colitis by suppressing intestinal stem cell renewal. Cell Stem Cell 29: 1366-1381.e9, 2022.
12. Ding L, Yang L, Wang Z and Huang W: Bile acid nuclear receptor FXR and digestive system diseases. Acta Pharm Sin B 5: 135-144, 2015.
13. Li T, Ding N, Guo H, Hua R, Lin Z, Tian H, Yu Y, Fan D, Yuan Z, Gonzalez FJ and Wu Y: A gut microbiota-bile acid axis promotes intestinal homeostasis upon aspirin-mediated damage. Cell Host Microbe 32: 191-208.e9, 2024.
14. Liu F, Yao Y, Wang Q, Zhang F, Wang M, Zhu C and Lin C: Nigakinone alleviates DSS-induced experimental colitis via regulating bile acid profile and FXR/NLRP3 signaling pathways. Phytother Res 37: 15-34, 2023.
15. Hou Q, Ye L, Liu H, Huang L, Yang Q, Turner JR and Yu Q: Lactobacillus accelerates ISCs regeneration to protect the integrity of intestinal mucosa through activation of STAT3 signaling pathway induced by LPLs secretion of IL-22. Cell Death Differ 25: 1657-1670, 2018.
16. Montgomery RK and Shivdasani RA: Prominin1 (CD133) as an intestinal stem cell marker: Promise and nuance. Gastroenterology 136: 2051-2054, 2009.
17. Bao W, You Y, Ni J, Hou H, Lyu J, Feng G, Wang Y, You K, Zhang S, Zhang L, *et al*: Inhibiting sorting nexin 10 promotes mucosal healing through SREBP2-mediated stemness restoration of intestinal stem cells. Sci Adv 9: eadh5016, 2023.
18. Yuan SN, Wang MX, Han JL, Feng CY, Wang M, Wang M, Sun JY, Li NY, Simal-Gandara J and Liu C: Improved colonic inflammation by nervonic acid via inhibition of NF-κB signaling pathway of DSS-induced colitis mice. Phytomedicine 112: 154702, 2023.
19. Zheng J, Zhang J, Zhou Y, Zhang D, Guo H, Li B and Cui S: Taurine alleviates experimental colitis by enhancing intestinal barrier function and inhibiting inflammatory response through TLR4/NF-κB signaling. J Agric Food Chem 72: 12119-12129, 2024.
20. Fujii Y, Yoshihashi K, Suzuki H, Tsutsumi S, Mutoh H, Maeda S, Yamagata Y, Seto Y, Aburatani H and Hatakeyama M: CDX1 confers intestinal phenotype on gastric epithelial cells via induction of stemness-associated reprogramming factors SALL4 and KLF5. Proc Natl Acad Sci USA 109: 20584-20589, 2012.
21. Wang MQ, Zhang KH, Liu FL, Zhou R, Zeng Y, Chen AL, Yu Y, Xia Q, Zhu CC and Lin CZ: Wedelolactone alleviates cholestatic liver injury by regulating FXR-bile acid-NF-κB/NRF2 axis to reduce bile acid accumulation and its subsequent inflammation and oxidative stress. Phytomedicine 122: 155124, 2024.
22. Parikh K, Antanaviciute A, Fawkner-Corbett D, Jagielowicz M, Aulicino A, Lagerholm C, Davis S, Kinchen J, Chen HH, Alham NK, *et al*: Colonic epithelial cell diversity in health and inflammatory bowel disease. Nature 567: 49-55, 2019.
23. Tran HTN, Ang KS, Chevrier M, Zhang X, Lee NYS, Goh M and Chen J: A benchmark of batch-effect correction methods for single-cell RNA sequencing data. Genome Biol 21: 12, 2020.
24. Vancamelbeke M, Vanuytsel T, Farré R, Verstockt S, Ferrante M, Van Assche G, Rutgeerts P, Schuit F, Vermeire S, Arijs I and Cleynen I: Genetic and transcriptomic bases of intestinal epithelial barrier dysfunction in inflammatory bowel disease. Inflamm Bowel Dis 23: 1718-1729, 2017.
25. Bjerrum JT, Hansen M, Olsen J and Nielsen OH: Genome-wide gene expression analysis of mucosal colonic biopsies and isolated colonocytes suggests a continuous inflammatory state in the lamina propria of patients with quiescent ulcerative colitis. Inflamm Bowel Dis 16: 999-1007, 2010.
26. Li K, Strauss R, Ouahed J, Chan D, Telesco S, Shouval DS, Canavan JB, Brodmerkel C, Snapper SB and Friedman JR: Molecular comparison of adult and pediatric ulcerative colitis indicates broad similarity of molecular pathways in disease tissue. J Pediatr Gastroenterol Nutr 67: 45-52, 2018.
27. Robinson MD, McCarthy DJ and Smyth GK: edgeR: A BIoconductor package for differential expression analysis of digital gene expression data. Bioinformatics 26: 139-140, 2010.
28. Love MI, Huber W and Anders S: Moderated estimation of fold change and dispersion for RNA-seq data with DESeq2. Genome Biol 15: 550, 2014.
29. Liu S, Wang Z, Zhu R, Wang F, Cheng Y and Liu Y: Three differential expression analysis methods for RNA sequencing: Limma, EdgeR, DESeq2. J Vis Exp, 2021.
30. Ritchie ME, Phipson B, Wu D, Hu Y, Law CW, Shi W and Smyth GK: Limma powers differential expression analyses for RNA-sequencing and microarray studies. Nucleic Acids Res 43: e47, 2015.
31. Langfelder P and Horvath S: WGCNA: An R package for weighted correlation network analysis. BMC Bioinformatics 9: 559, 2008.
32. Zhu L, Gibson P, Currle DS, Tong Y, Richardson RJ, Bayazitov IT, Poppleton H, Zakharenko S, Ellison DW and Gilbertson RJ: Prominin 1 marks intestinal stem cells that are susceptible to neoplastic transformation. Nature 457: 603-607, 2009.
33. Barker N, van Es JH, Kuipers J, Kujala P, van den Born M, Cozijnsen M, Haegebarth A, Korving J, Begthel H, Peters PJ and Clevers H: Identification of stem cells in small intestine and colon by marker gene Lgr5. Nature 449: 1003-1007, 2007.
34. Liu T, Zhang L, Joo D and Sun SC: NF-κB signaling in inflammation. Signal Transduct Target Ther 2: 17023, 2017.
35. Rai A, Kapoor S, Singh S, Chatterji BP and Panda D: Transcription factor NF-κB associates with microtubules and stimulates apoptosis in response to suppression of microtubule dynamics in MCF-7 cells. Biochem Pharmacol 93: 277-289, 2015.
36. Yui S, Azzolin L, Maimets M, Pedersen MT, Fordham RP, Hansen SL, Larsen HL, Guiu J, Alves MRP, Rundsten CF, *et al*: YAP/TAZ-dependent reprogramming of colonic epithelium links ECM remodeling to tissue regeneration. Cell Stem Cell 22: 35-49.e7, 2018.

37. Zeuner A, Todaro M, Stassi G and De Maria R: Colorectal cancer stem cells: From the crypt to the clinic. Cell Stem Cell 15: 692-705, 2014.
38. Chen WD, Wang YD, Zhang L, Shiah S, Wang M, Yang F, Yu D, Forman BM and Huang W: Farnesoid X receptor alleviates age-related proliferation defects in regenerating mouse livers by activating forkhead box m1b transcription. Hepatology 51: 953-962, 2010.
39. Seitz CS, Lin Q, Deng H and Khavari PA: Alterations in NF-kappaB function in transgenic epithelial tissue demonstrate a growth inhibitory role for NF-kappaB. Proc Natl Acad Sci USA 95: 2307-2312, 1998.
40. Biton M, Haber AL, Rogel N, Burgin G, Beyaz S, Schnell A, Ashenberg O, Su CW, Smillie C, Shekhar K, *et al*: T helper cell cytokines modulate intestinal stem cell renewal and differentiation. Cell 175: 1307-1320.e22, 2018.